SNOW WATER EQUIVALENT ESTIMATES IN THE HINDU KUSH AND THE SIERRA NEVADA USING PASSIVE MICROWAVE AND RECONSTRUCTION

Edward H. Bair [1,2], Jeff Dozier[3], Karl Rittger[4], Carrie Voyuvich[1], and Robert E. Davis[1]

ABSTRACT

Accurate measurement of spatially distributed snow water equivalent (SWE) in mountain watersheds is perhaps the most significant problem in snow hydrology. We examine SWE measurements from two techniques. The first uses passive microwave estimates, provided by the National Snow and Ice Data Center, from the AMSR-E sensor aboard the Aqua satellite. Passive microwave (PM) has been used to estimate SWE for decades, and while it is subject to numerous problems, it is the only source of global real-time SWE estimates. Recently, SWE Reconstruction has been shown to be accurate at estimating basin-wide SWE in the Sierra Nevada. Reconstruction combines a melt model with snow covered area measurements to retroactively build the snowpack, from disappearance back to its peak. Reconstruction can only be used retrospectively, so it cannot be used to estimate today's SWE. Thus, we use Reconstruction of prior water years to better understand the strengths and weaknesses of PM SWE estimates. Our test case is California's Sierra Nevada, where we have full natural flow estimates and a large network of SWE sensors for comparison. Our application area is the Hindu Kush range in Afghanistan, where there are neither stream flow nor ground-based SWE measurements. Both regions are snowmelt dominated and subject to drought. Using annual SWE estimates from Reconstruction for verification, our results show that annual PM SWE estimates are biased in California and Afghanistan. In California, SWE estimates from AMSR-E are too low, by up to 10×. In the Amu Darya, one of the largest basins in Afghanistan, SWE estimates are too low by about 2×, while in 5/8 basins, PM SWE estimates are consistently too high. In terms of ranks, PM performs poorly, having low Spearman rank correlation coefficients. An exception is the Amu Darya, where the Spearman correlation coefficient is 0.81 for the eight years studied. We examine potential sources of error. Consistent with previous studies, we find that PM error is caused by shallow snow, deep snow, and forest cover. The explanation for the relatively low bias in SWE and relatively high correlation of rank for the Amu Darya appears to be a snowpack that was neither shallow nor exceptionally deep in a region that is nearly devoid of tree cover. (KEYWORDS: reconstruction, passive microwave, AMSR-E, Afghanistan, Sierra Nevada)

INTRODUCTION

Accurate estimates of snow water equivalent (SWE) in mountain watersheds are a longstanding and unsolved problem. Operational models have high uncertainty, and this uncertainty has high costs for water users. For instance, April to July runoff forecasts for the American River in California's Sierra Nevada have an 18% error on average, and sometimes exceed 100% (Dozier, 2011). Uncertainty stems from the heterogeneous nature of mountain snow. Spectroscopic techniques using satellite-based imagery in the visible and near-IR bands have been successful at mapping snow covered area (SCA) at sub-pixel resolution (e.g., Rosenthal and Dozier, 1996; Painter et al., 2009). Measurements of SCA are combined with a Reconstruction technique (Martinec and Rango, 1981), which has successfully modeled SWE in large basins in the Rocky Mountains (Molotch, 2009) and the Sierra Nevada (Rittger, 2012). The main advantage of Reconstruction is that it provides spatially resolved SWE estimates without the need for extensive ground based observations. The biggest disadvantages are that Reconstruction can only be run retroactively after snow disappears, and that it is only suitable for areas with little accumulation during the melt season. Alternatively, passive microwave (PM) sensors offer real-time global SWE estimates but suffer from a number of issues caused by: signal loss in wet snow (Chang, 2000), saturation in deep snow (e.g. > 250 mm SWE, Takala et al., 2011), decreasing SWE with increasing forest fraction (Nolin, 2010; Tedesco and Narvekar, 2010), and SWE overestimation in the presence of large grains such as depth and surface hoar (Derksen et al., 2005; Durand et al., 2011).

Paper presented Western Snow Conference 2014
[1] US Army Corps of Engineers Cold Regions Research and Engineering Laboratory, Hanover, NH
[2] Earth Research Institute, University of California, Santa Barbara, nbair@eri.ucsb.edu
[3] Bren School of Environmental Science and Management, University of California, Santa Barbara
[4] National Snow and Ice Data Center, Boulder, CO

STUDY AREAS

Sierra Nevada

The Sierra Nevada (Figure 1) receives heavy winter precipitation and is marked by seasonal summer drought. Precipitation from October through May accounts for 95% of annual precipitation (NOAA National Climatic Data Center, 2014). Limited accumulation during the snowmelt season makes the Sierra Nevada an excellent area for Reconstruction. The highest mountains are about 4,400 m. The range, especially the western slopes, is densely forested (Figure 1b), with areas of seasonal snowcover having about 70% forest cover on average (Raumann and Soulard, 2007).

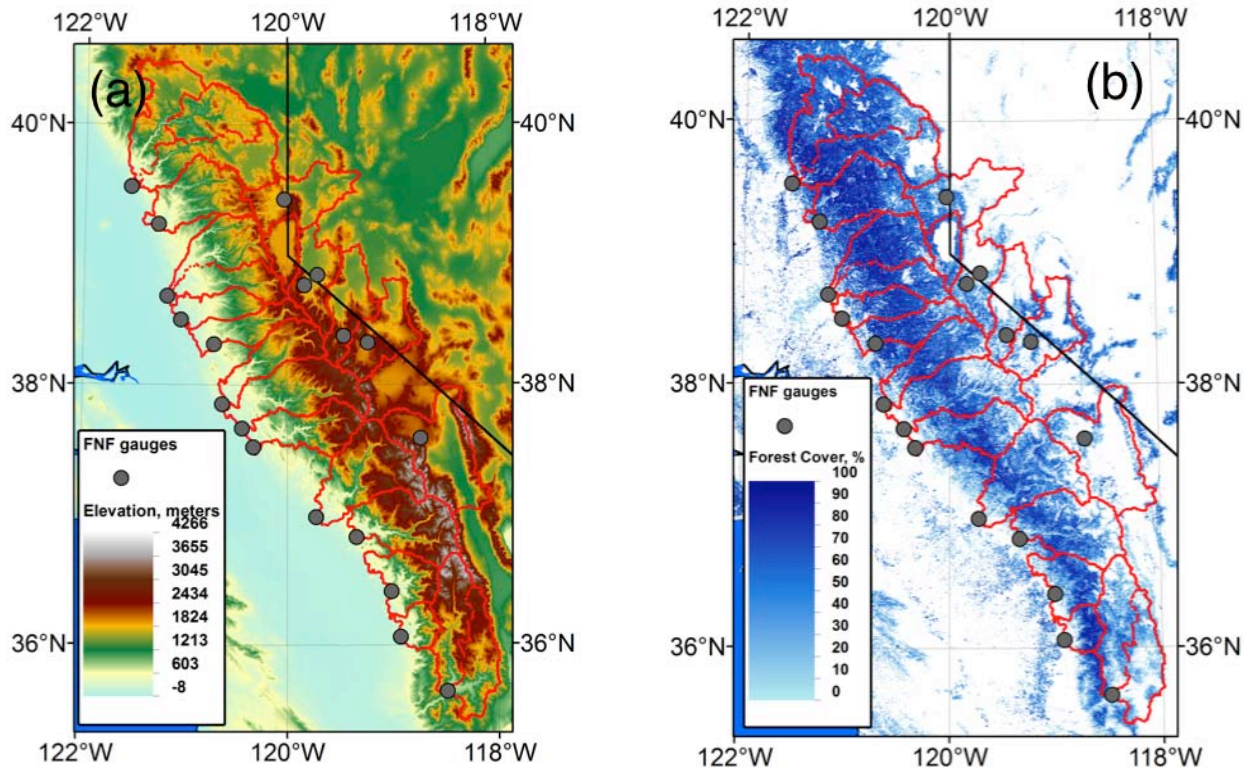

Figure 1. (a, left) Sierra Nevada HUC 8 basins, gauges where full natural flow is measured, and elevation from the Shuttle Radar Topography Mission. (b, right) Same area, but showing forest cover from the National Land Cover Database.

Hindu Kush

Like the Sierra Nevada, the Hindu Kush range in Afghanistan (Figure 2) is marked by seasonal drought with little accumulation during the melt season. Climate data from the Air Force Combat Climatology Center show that around 97% of annual precipitation in Afghanistan falls from October through May. Generally, the Hindu Kush is colder and drier than the Sierra Nevada. The highest mountains are also taller, with some peaks approaching 7,500 m. Historically, in Afghanistan's arid climate, about 5% of the country's land area was forested. Decades of war, illegal logging, and a lack of replanting have reduced forest cover to only 2% (United Nations, 2009). Note, because of vast differences in area between HUC8 basins in the Sierra and basins in the Hindu Kush (Table 1), the aggregate of all the HUC8 basins in the Sierra together approximate one basin in the Hindu Kush.

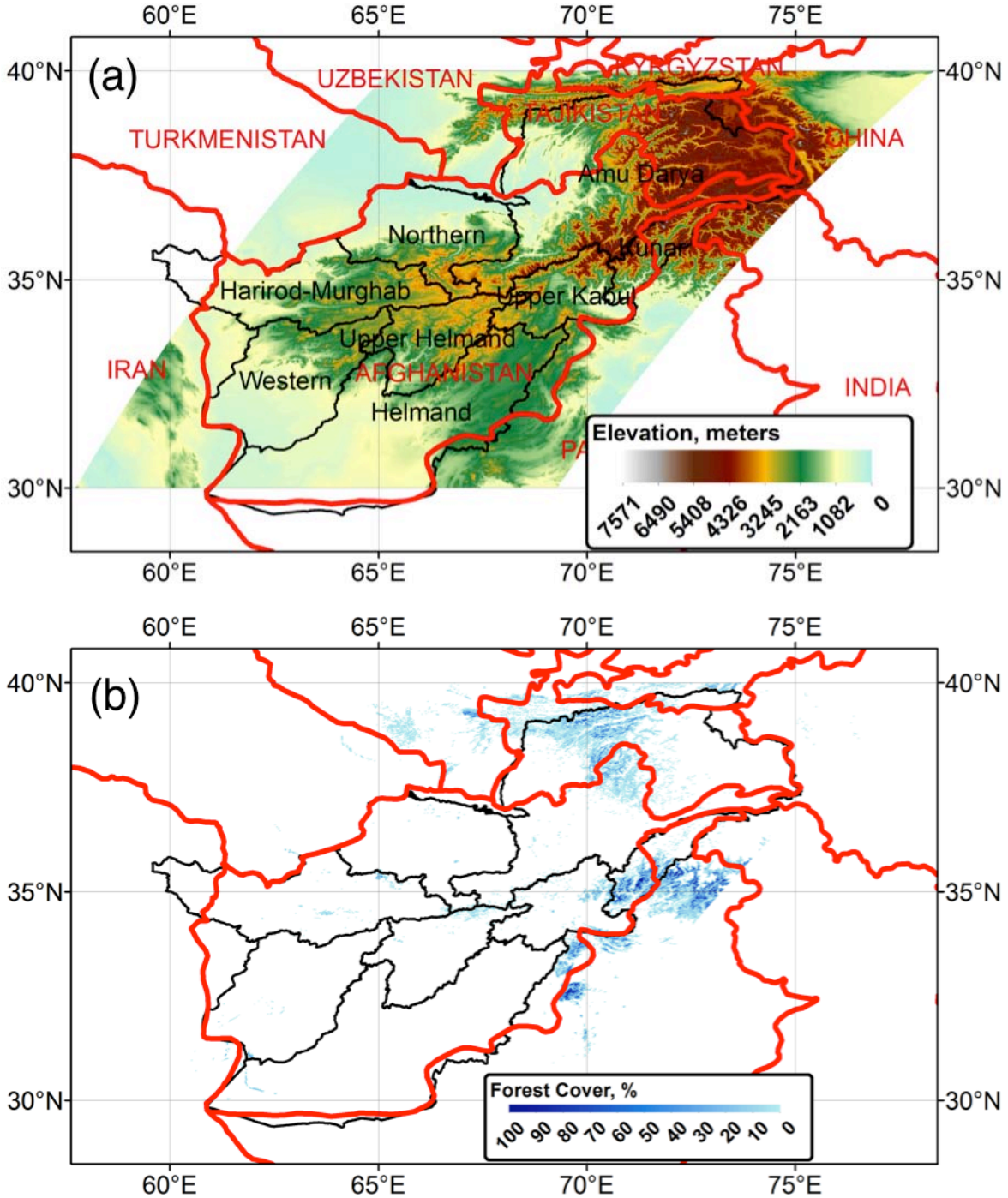

Figure 2. (a, top) Afghanistan basins, surrounding countries, and elevation from ASTER Global DEM. (b, bottom) Same area, but showing forest cover from Geocover.

Region	Name	Area, km^2
Sierra Nevada	19 modified HUC8 basins	53,593
Afghanistan	Amu Darya	207,379
	Harirod-Murghab	77,891
	Helmand	201,102
	Upper Kabul	42,170
	Kunar	25,836
	Northern	70,891
	Western	85,350
	Upper Helmand	46,876

Table 1. List of basins and areas

METHODS

Reconstruction

Reconstruction uses an energy balance approach. For each pixel, from date of peak SWE through the disappearance of snow in a satellite image, Reconstruction retrospectively builds the snow cover by calculating the amount of snow melted at each daily time step *j* (Molotch, 2009):

$$\mathrm{SWE_n} = \mathrm{SWE_0} - \sum_{j=1}^{n} M_j \qquad [1]$$

SWE_n and SWE_0 are the SWE at days *n* and 0, and M_j is the melted SWE. Knowing the value of *n* when $SWE_n = 0$ (i.e. when SCA = 0) allows the back-calculation of the initial SWE_0. For the Sierra Nevada, the date of SWE_0 was computed by interpolating the peak SWE date for each year from snow pillow measurements (Rittger, 2012). For each pixel in the Hindu Kush, the peak SWE date was computed by finding the first day D_1 where melt was ≥ 19 mm/day for 3 consecutive days. The average date between D_1 and D_2, the day with maximum melt, was selected as the peak SWE date. The 19 mm/day melt threshold over 3 consecutive days was chosen by running simulations on the Sierra Nevada reconstructed SWE to match a known peak SWE date at a snow pillow. For most pixels, this threshold translated to a date immediately prior to the onset of a sustained multi-day or multi-week melt. Melted SWE is the product of the potential melt $P_{,j}$ and the fractional snowcover f_{SCA}:

$$\mathrm{M_j} = \mathrm{P_j} \times \mathrm{f_{sca}} \qquad [2]$$

The potential melt is estimated with a combined net radiation and degree day model (Kustas et al., 1994):

$$\mathrm{P_j} = \mathrm{m_q R_d} + \mathrm{B_r T_d} \qquad [3]$$

The energy balance terms are: m_q, an energy to radiation melt factor and R_d, the mean daily net radiation. The degree day terms are: B_r, a degree day melt factor, and T_d, the average daily air temperature if > 0 ºC or zero otherwise. The final Reconstruction product was projected into a California Albers Equal Area grid with 0.5 km^2 pixels for the Sierra Nevada and a sinusoidal grid, also with 0.5 km^2 pixels, for Afghanistan.

SNODAS and Interpolation

In the Sierra Nevada, we also used SWE estimates from SNODAS (SNOw Data Assimilation System, National Operational Hydrologic Remote Sensing Center, 2004) and snow pillow interpolation (Fassnacht et al., 2003). SNODAS results come directly from the National Snow and Ice Data Center and are available daily. The snow pillow interpolation is a research product. One of its key inputs, time and spaced smoothed SCA (Dozier et al., 2008), is not yet produced operationally.

Passive Microwave

For regions with austere infrastructure, we cannot use models that rely on ground-based observations. In the Hindu Kush, we used satellite-derived measurements of SWE from PM emission through the snow (Daly et al., 2012). Specifically, these measurements came from the AMSR-E and SSM/I satellites. In this study, we used SWE estimates from the AMSR-E satellite. AMSR-E stopped functioning October 2011, but global SWE products are available from

SSM/I and the recently launched Japanese AMSR2. PM pixel areas are 2500× larger than those in Reconstruction, Interpolation, and SNODAS (25.0 vs. 0.5 km^2) and suffer from a variety of complicating factors such as forests, wet snow, and rough terrain (Dong et al., 2005; Vander Jagt et al., 2013). Among other problems, these complicating factors cause noise in the AMSR-E signal, which we smoothed in two steps: 1) we found peaks over a 7-day interval, and 2) we interpolated between peaks with splines. Additionally, we reprojected the AMSR-E SWE data into 10 km^2 pixels in a California Albers or sinusoidal grid to match the Reconstruction data. The sinusoidal grid was chosen because it is the format used by MODIS, from which our SCA estimates originated (MODSCAG, Painter et al., 2009). We choose 10 km^2 pixels (rather than the original 25 km^2 pixels) to make comparisons with the much smaller 0.5 km^2 pixels in Reconstruction. We found that the 10 km^2 pixels eliminated some of the sharp boundaries between areas with and without SWE, which would have compared poorly.

We also set AMSR-E SWE values above 250 mm to equal 250 mm, since these high values are likely spurious. Last, we took the 90th percentile of SWE for each pixel to estimate annual maximums. We choose the 90th percentile rather than the maximum SWE value for each pixel to reduce spuriously high SWE spikes that appeared as spots. Using the 90th percentile reduces the occurrence of these spots dramatically while still giving a close estimate of annual max in the areas where the spots did not appear.

Full Natural Flow

In the Sierra Nevada, we include spring full natural flow (FNF) as an independent measure of water year rank. Full natural flow is the measured streamflow adjusted for reservoir evaporation and withdrawals upstream of the gauge. Spring full natural flow is the summed (April 1 - June 30) flow for 19 gauges in the Sierra Nevada where full natural flow is calculated. These gauges collect runoff from a total area of 53,593 km^2. This area was mapped using the total area of 19 modified HUC8 basins where areas in each basin that were below the flow gauges were removed (Rittger, 2012).

We expect the ranks of the FNF data to match the ranks of the SWE estimates because SWE has the most influence over FNF variability. Ideally, the FNF data would be adjusted to remove rainfall. For this study, we find that using the FNF data without adjustment is acceptable, as the April 1-June 30 period in the Sierra is usually quite dry. Precipitation records from the California Data Exchange Center (http://cdec.water.ca.gov) show that this period only accounts for 10-13 cm or 8% to 10% of annual precipitation.

RESULTS

Sierra Nevada

Reconstruction consistently produces more SWE than any other method and has the highest R^2 in comparison with April to July full natural flow (Figure 3). In the Sierra, losses due to sublimation and evapotranspiration are 20-60% of total SWE (Kattelmann and Elder, 1991; Hunsaker et al., 2012), so one would expect SWE to be 120-160% greater than FNF. In most years, snow pillow interpolation and SNODAS also compare well with FNF estimates and have slightly higher Spearman rank correlation coefficients than Reconstruction (Table 2).

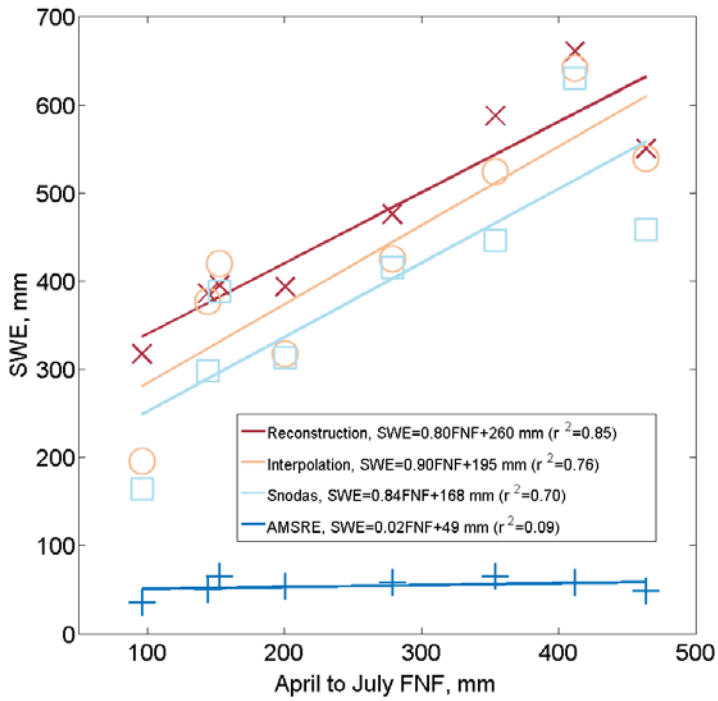

Figure 3. Sierra annual SWE estimates from four methods compared to April to July Full Natural Flow (FNF). SWE is normalized by basin area. Regression coefficients and R^2 values were computed for each method. Water years 2004-2011 were used.

In general, Reconstruction, Interpolation, and SNODAS compare well with FNF estimates both in annual SWE and rank. In contrast, AMSR-E compares poorly to FNF estimates both in annual SWE and rank. AMSR-E SWE estimates are 5-11x smaller than those from the other methods. The rank correlation coefficient between AMSR-E and FNF is only 0.25, compared with 0.90-0.95 for the other methods.

	Reconstruction	Interpolation	SNODAS	AMSR-E	FNF
Reconstruction	1.00				
Interpolation	0.95	1.00			
SNODAS	0.98	0.98	1.00		
AMSR-E	0.55	0.40	0.42	1.00	
FNF	0.90	0.90	0.95	0.25	1.00

Table 2. Spearman rank correlation coefficient matrix for different SWE products.

Hindu Kush

In Afghanistan, we only compared AMSR-E SWE estimates with Reconstruction (Figure 4) since SNODAS, full natural flow, and snow pillow data are not available. Those methods rely on ground based measurements, whereas Reconstruction does not require ground based measurements, making it particularly well suited for the Hindu Kush's austere landscape. The results range greatly depending on the basin. For the Amu Darya (Figure 4a), the R^2 value (0.64) approaches that of SNODAS in the Sierra Nevada (0.70). In six other basins (Figure 4b,d-h), R^2 is 0.12 or less. In some basins (Figure 4b,c,f-h), AMSR-E SWE is greater than Reconstruction SWE in all years. In terms of ranks, the Amu Darya has a Spearman correlation coefficient with Reconstruction of 0.81 (Figure 5), which is lower than Interpolation and SNODAS' rank correlation to Reconstruction in the Sierra (0.95 and 0.98, respectively), but far higher than the AMSR-E rank correlation with Reconstruction in the Sierra (0.55).

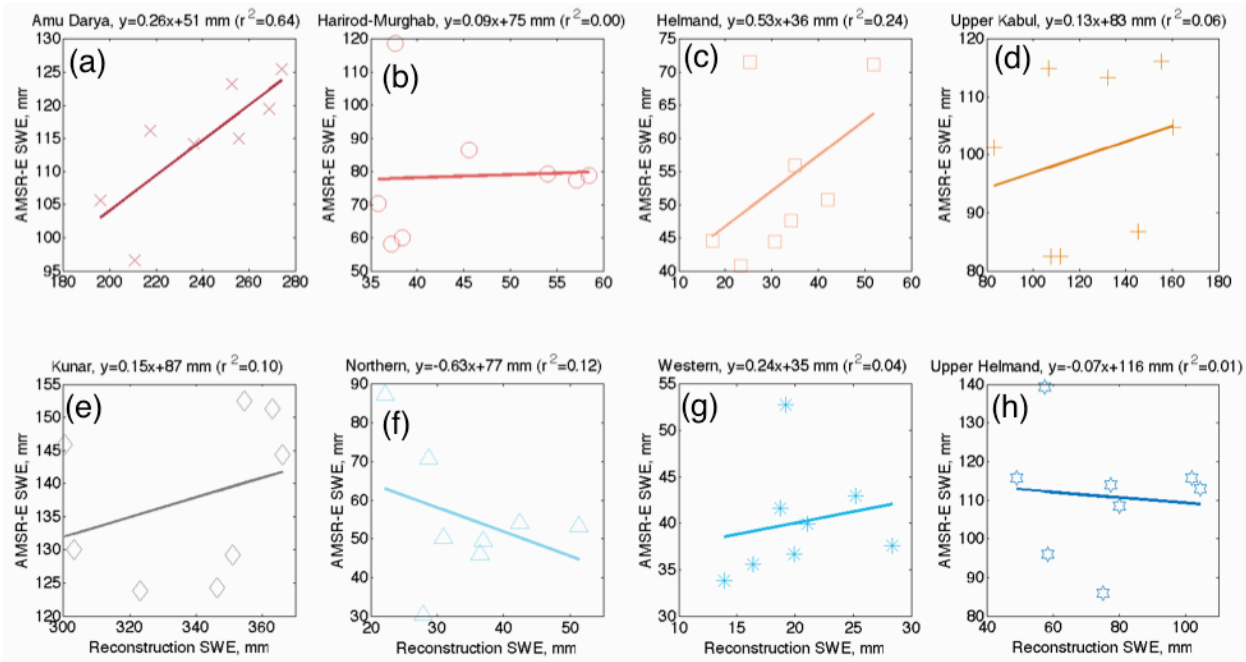

Figure 4. a-h Annual AMSR-E SWE vs Reconstruction SWE for 8 basins in Afghanistan. SWE is normalized by basin area. Water years 2004-2011 are shown.

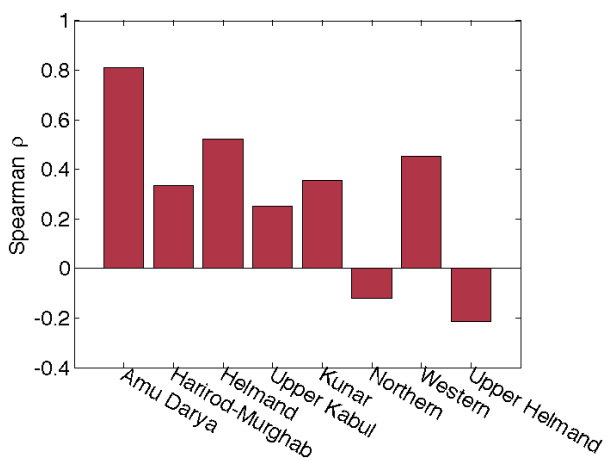

Figure 5. Spearman correlation coefficient between annual AMSR-E and Reconstruction SWE for eight basins in Afghanistan, 2004-2011.

DISCUSSION

To investigate sources of error in the AMSR-E SWE, we examined regressions between AMSR-E and Reconstruction in the Sierra Nevada and Hindu Kush (e.g. Figure 6). For these comparisons, the Reconstruction data were upscaled to match the AMSR-E pixel size (10 km^2). For some reason, AMSR-E misses more SWE in the Sierra Nevada and detects more SWE in the Amu Darya compared to Reconstruction. We suggest this apparent loss of SWE is caused by differences in forest cover. In a 2-d histogram of reconstructed SWE and forest fraction for the Sierra (Figure 7a), SWE is distributed throughout the forest cover range. Conversely, AMSR-E SWE (Figure 7b) decreases with increasing forest cover, suggesting that detection efficiency decreases with forest cover. A trend of increasing

underestimation of SWE with increasing forest fraction has been found in other studies on AMSR-E SWE

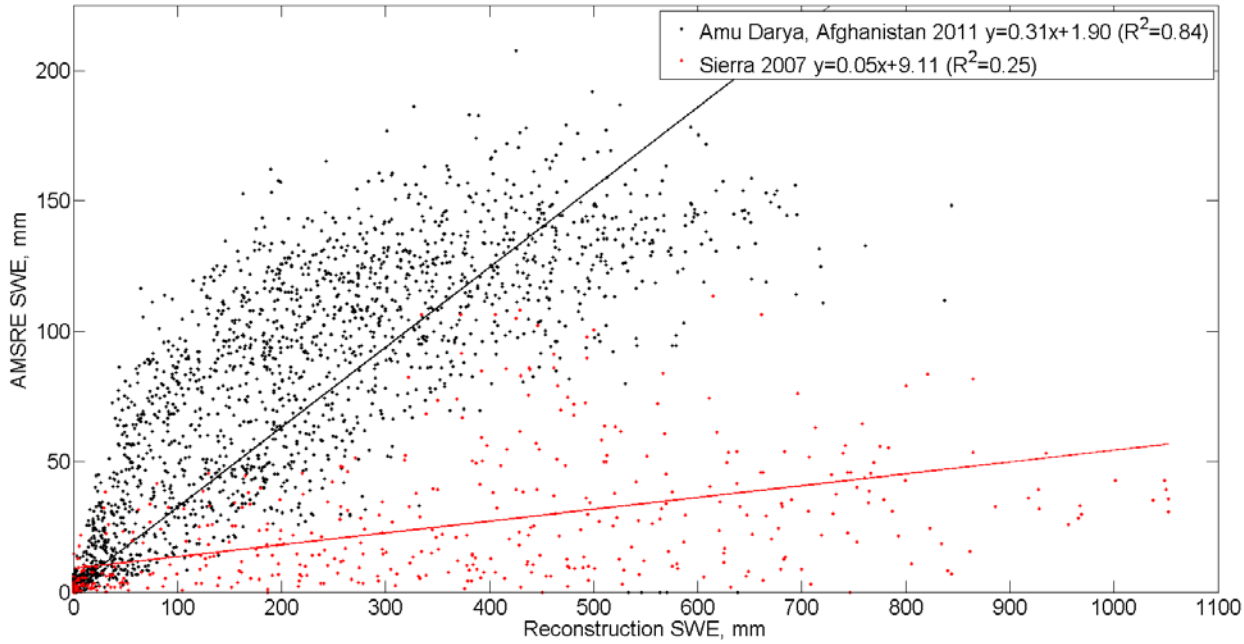

Figure 6. AMSR-E SWE vs. Reconstruction SWE for two drought years: 2007 in the Sierra and 2011 in Afghanistan. Each point is a 10 km^2 pixel.

(Foster et al., 1997; Tedesco and Narvekar, 2010). The AMSR-E SWE algorithm (Chang, 2000) attempts to compensate for decreased brightness temperatures of snow in forested areas using a linear mixture model, but the SWE signal likely becomes so attenuated under a dense canopy that the mixture model fails to give accurate results.

In comparison, the 2-d histogram shape of SWE vs. forest cover for Reconstruction in the Amu Darya (Figure 7c) is replicated by AMSR-E (Figure 7d). Although AMSR-E is detecting less SWE than Reconstruction, there is no loss of SWE as forest cover increases. The magnitude of AMSR-E SWE is lower than the reconstructed SWE by 2x, but that is less of an underestimate than in the Sierra, where AMSR-E SWE is smaller by 5-11x. We suggest that the lack of tree cover in the Amu Darya explains why AMSR-E estimates are closer to those from Reconstruction. The Amu Darya forest fraction peaks at 30 %, compared to 80% in the Sierra, and many snow covered pixels have 0% forest cover.

Also, the Amu Darya has a snowpack that appears to be deep enough to overcome thin snowpack and depth hoar issues, which seem to plague many of the other basins in Afghanistan with shallower snowpacks. Yet the snowpack in the Amu Darya is not as deep as the Sierra snowpack. The reconstructed snowpack, normalized by basin area, for the Amu Darya ranges from 196-274 mm, depending on the year (Figure 4a). Most years are below the 250 mm AMSR-E saturation limit. In comparison, the reconstructed Sierra snowpack ranges from 317-550 mm (Figure 3), thus all years are above the 250 mm saturation limit. Reconstructed SWE in the other Afghanistan basin with a deep snowpack, the Kunar, range from 300-266 mm, also above the AMSR-E saturation limit for all years.

CONCLUSIONS

We examined two techniques for annual SWE estimation in the Hindu Kush and the Sierra Nevada. Reconstruction in the Sierra matches well with spring full natural flow volumes and ranks. One major advantage Reconstruction has over SNODAS and snow pillow interpolation is that it does not require ground-based snow observations. Thus, we were able to reconstruct snow in Afghanistan from 2004-2011 with, what we predict to be, similar accuracy to the Sierra. The main disadvantage of Reconstruction is that it can only be done retrospectively, since one must know when SCA goes to zero for each pixel.

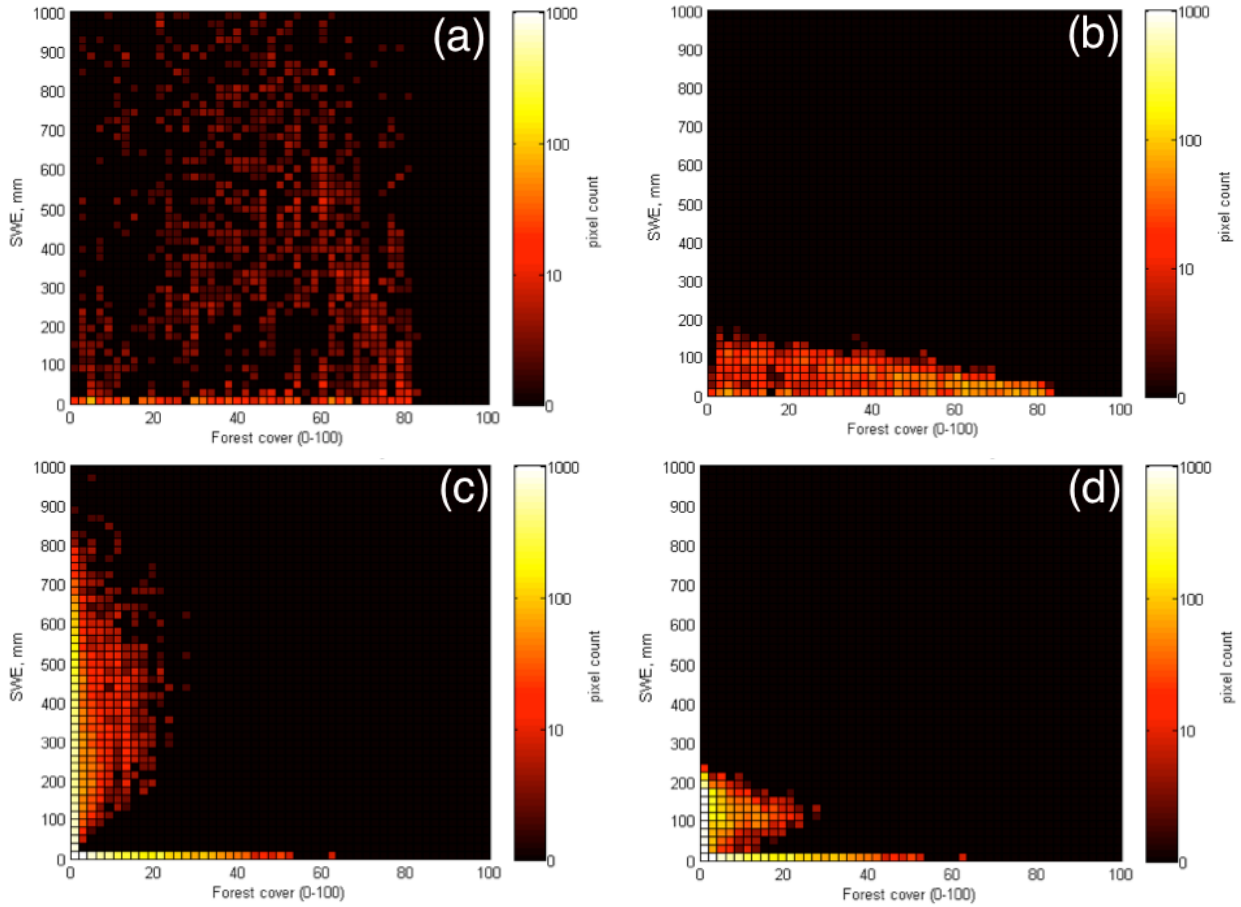

Figure 7. a-d Two-dimensional histograms of annual SWE vs. forest cover for (a) Reconstruction in the Sierra, (b) AMSR-E in the Sierra, (c) Reconstruction in the Amu Darya, and (d) AMSR-E in the Amu Darya. Histograms are from annual SWE values from 2004-2011.

Passive microwave is the only global SWE product available in real-time. It suffers from many issues, but its performance depends greatly on the study area. We tested the accuracy of annual SWE estimates made from AMSR-E passive microwave data in the Sierra and Hindu Kush using reconstructed annual SWE as our verification. In general, AMSR-E performed poorly in the Sierra. Annual SWE estimates were too small by up to 10× and the ranks did not match well with full natural flows or any of the other methods. We suggest this poor performance was caused primarily by dense forest cover, but also by a snowpack deeper than the AMSR-E saturation threshold.

In 7 of 8 basins in Afghanistan, AMSR-E also performed poorly in terms of SWE volumes and rank order. Unlike the Sierra, in 5 of 8 basins AMSR-E annual SWE was greater than reconstructed SWE in all years. These basins tended to have thin snowpacks, associated with large grains caused by high temperature gradients (depth hoar). Because the passive microwave SWE retrieval coefficients are sensitive to grain size, unusually large grains can lead to overestimation of SWE because of increased absorption and scattering. Large areas with thin snowpacks that may have been predominately composed of depth hoar may explain the AMSR-E SWE overestimate in Afghanistan.

An important exception is the Amu Darya, one of the largest basins in the Hindu Kush. The R^2 for the Amu Darya against reconstructed SWE was 0.64, close to the R^2 value (0.70) for SNODAS/Reconstruction in the Sierra. The Spearman correlation coefficient between AMSR-E SWE and Reconstruction for the Amu Darya was 0.81, higher than all other basins in Afghanistan and higher than its rank correlation with Reconstruction in the Sierra (0.55). We suggest that the Amu Darya is an ideal basin for passive microwave SWE estimates. The Amu Darya is large (over 200,000 km^2), thus it is suitable to passive microwave footprints. It has a snowpack that is deep enough to overcome the shallow snowpack problems associated with AMSR-E that plague other basins in the Hindu Kush. Most importantly, the Amu Darya has little forest cover, meaning that the passive microwave signal from the snow is not heavily attenuated by tree

cover. We conclude that AMSR-E SWE estimates (and likely those from AMSR-2 since its sensor and algorithm are similar to AMSR-E) are relatively accurate for large areas with moderate snowpacks and limited forest cover.

REFERENCES

Chang, A.T.C. 2000. Algorithm Theoretical Basis Documnet (ATBD) for the AMSR-E Snow Water Equivalent Algorithm. NASA Goodard Space Flight Center, Greenbelt, Maryland, pp. 49.

Daly, S.F., C.M. Vuyovich, E.J. Deeb, S.D. Newman, T.B. Baldwin, and J.J. Gagnon. 2012. Assessment of the snow conditions in the major watersheds of Afghanistan using multispectral and passive microwave remote sensing. Hydrological Processes, 26(17): 2631-2642, doi: 10.1002/hyp.9367.

Derksen, C., A. Walker, and B. Goodison. 2005. Evaluation of passive microwave snow water equivalent retrievals across the boreal forest/tundra transition of western Canada. Remote Sensing of Environment, 96(3–4): 315-327, doi: http://dx.doi.org/10.1016/j.rse.2005.02.014.

Dong, J., J.P. Walker, and P.R. Houser. 2005. Factors affecting remotely sensed snow water equivalent uncertainty. Remote Sensing of Environment, 97(1): 68-82, doi: 10.1016/j.rse.2005.04.010.

Dozier, J. 2011. Mountain hydrology, snow color, and the fourth paradigm. Eos, Transactions American Geophysical Union, 92(43): 373-374, doi: 10.1029/2011eo430001.

Dozier, J., T.H. Painter, K. Rittger, and J. Frew. 2008. Time-space continuity of daily maps of fractional snow cover and albedo from MODIS. Advances in Water Resources, 31(11): 1515-1526, doi: 10.1016/j.advwatres.2008.08.011.

Durand, M., E.J. Kim, S.A. Margulis, and N.P. Molotch. 2011. A First-Order Characterization of Errors From Neglecting Stratigraphy in Forward and Inverse Passive Microwave Modeling of Snow. Geoscience and Remote Sensing Letters, IEEE, 8(4): 730-734, doi: 10.1109/LGRS.2011.2105243.

Fassnacht, S.R., K.A. Dressler, and R.C. Bales. 2003. Snow water equivalent interpolation for the Colorado River Basin from snow telemetry (SNOTEL) data. Water Resources Research, 39, doi: 10.1029/2002wr001512.

Foster, J.L., A.T.C. Chang, and D.K. Hall. 1997. Comparison of Snow Mass Estimates from a Prototype Passive Microwave Snow Algorithm, a Revised Algorithm and a Snow Depth Climatology. Remote Sensing of Environment, 62: 132-142.

Hunsaker, C.T., T.W. Whitaker, and R.C. Bales. 2012. Snowmelt Runoff and Water Yield Along Elevation and Temperature Gradients in California's Southern Sierra Nevada1. JAWRA Journal of the American Water Resources Association, 48(4): 667-678, doi: 10.1111/j.1752-1688.2012.00641.x.

Kattelmann, R. and K. Elder. 1991. Hydrologic characteristics and water balance of an Alpine Basin in the Sierra Nevada. Water Resources Research, 27(7): 1553-1562, doi: 10.1029/90wr02771.

Kustas, W.P., A. Rango, and R. Uijlenhoet. 1994. A simple energy budget algorithm for the snowmelt runoff model. Water Resources Research, 30(5): 1515-1527, doi: 10.1029/94wr00152.

Martinec, J., and A. Rango. 1981. Areal distribution of snow water equivalent evaluated by snow cover monitoring. Water Resources Research, 17(5): 1480-1488, doi: 10.1029/WR017i005p01480.

Molotch, N.P. 2009. Reconstructing snow water equivalent in the Rio Grande headwaters using remotely sensed snow cover data and a spatially distributed snowmelt model. Hydrological Processes, 23(7): 1076-1089, doi: 10.1002/hyp.7206.

National Operational Hydrologic Remote Sensing Center. 2004. Snow Data Assimilation System (SNODAS) Data Products at NSIDC. National Snow and Ice Data Center, Boulder, CO USA.

NOAA National Climatic Data Center. 2014. Climate at a Glance, Time Series data.
Nolin, A., 2010. Recent advances in remote sensing of seasonal snow. Journal of Glaciolgy, 56(200): 1141-1150.

Painter, T.H., K. Rittger, C. McKenzie, R.E. Davis, and J. Dozier. 2009. Retrieval of subpixel snow-covered area, grain size, and albedo from MODIS. Remote Sensing of Environment, 113: 868–879, doi: 10.1016/j.rse.2009.01.001.

Raumann, C.G., and C.E. Soulard. 2007. Land Cover Trends in the Sierra Nevada Ecoregion. U.S. Geolocial Survey Scientific Investigations Report, pp. 29.

Rittger, K. 2012. Spatial estimates of snow water equivalent in the Sierra Nevada. Ph.D. Thesis, Unversity of California, Santa Barbara, Santa Barbara, 225 pp.

Rosenthal, W., and J. Dozier. 1996. Automated mapping of montane snow cover at subpixel resolution from the Landsat Thematic Mapper. Water Resources Research, 32(1): 115-130, doi: 10.1029/95WR02718.

Takala, M., K. Luojus, J. Pulliainen, C. Derksen, J. Lemmetyinen, J.-P. Kärnä, J. Koskinen, and B. Bojkov. 2011. Estimating northern hemisphere snow water equivalent for climate research through assimilation of space-borne radiometer data and ground-based measurements. Remote Sensing of Environment, 115(12): 3517-3529, doi: http://dx.doi.org/10.1016/j.rse.2011.08.014.

Tedesco, M., and P.S. Narvekar. 2010. Assessment of the NASA AMSR-E SWE Product. Selected Topics in Applied Earth Observations and Remote Sensing, IEEE Journal of, 3(1): 141-159, doi: 10.1109/JSTARS.2010.2040462.
United Nations, 2009. United Nations Environment Programme in Afghanistan, pp. 36.

Vander Jagt, B.J., M.T. Durand, S.A. Margulis, E.J. Kim, and N.P. Molotch. 2013. The effect of spatial variability on the sensitivity of passive microwave measurements to snow water equivalent. Remote Sensing of Environment, 136(0): 163-179, doi: 10.1016/j.rse.2013.05.002.